
TRANSFERRING VISUAL EXPLAINABILITY OF SELF-EXPLAINING MODELS THROUGH TASK ARITHMETIC

A PREPRINT

Yuya Yoshikawa
STAIR Lab, Chiba Institute of Technology
yoshikawa@stair.center

Ryotaro Shimizu
ZOZO Research
ryotaro.shimizu@zozo.com

Takahiro Kawashima
ZOZO Research
takahiro.kawashima@zozo.com

Yuki Saito
ZOZO Research
yuki.saito@zozo.com

July 8, 2025

ABSTRACT

In scenarios requiring both prediction and explanation efficiency for image classification, self-explaining models that perform both tasks in a single inference are effective. However, their training incurs substantial labeling and computational costs. This study aims to tackle the issue by proposing a method to transfer the visual explainability of self-explaining models, learned in a source domain, to a target domain based on a task arithmetic framework. Specifically, we construct a self-explaining model by extending image classifiers based on a vision-language pretrained model. We then define an *explainability vector* as the difference between model parameters trained on the source domain with and without explanation supervision. Based on the task arithmetic framework, we impart explainability to a model trained only on the prediction task in the target domain by applying the explainability vector. Experimental results on various image classification datasets demonstrate that, except for transfers between some less-related domains, visual explainability can be successfully transferred from source to target domains, improving explanation quality in the target domain without sacrificing classification accuracy. Furthermore, we show that the explainability vector learned on a large and diverse dataset like ImageNet, extended with explanation supervision, exhibits universality and robustness, improving explanation quality on nine out of ten different target datasets. We also find that the explanation quality achieved with a single model inference is comparable to that of Kernel SHAP, which requires 150 model inferences.

1 Introduction

Visual explainability, which provides human-understandable explanations for the classification results of prediction models, is important for various applications, such as medical image diagnosis [1], autonomous driving [2], manufacturing [3], cybersecurity [4], and model debugging [5].

Although explanations provide valuable insights to users, generating them often incurs significantly higher computational costs compared to performing prediction alone. When a trained model is already available, visual explanations can be generated using post-hoc explanation methods, such as SHAP [6] and Grad-CAM [7]. However, generating an explanation for a single image with SHAP typically requires at least hundreds of model inferences, and computing Grad-CAM necessitates calculating gradients of the model’s parameters, which requires resources for backward computation. Such computational challenges can be addressed by using *self-explaining models*, which are designed to perform both prediction and explanation at a single inference [8, 9]. Although self-explaining models are very efficient in the inference phase, their training incurs high computational costs due to the need to create ground-truth explanation data for user-desired explanations [10] or the requirement for numerous model forward computations to learn these explanations [11].

The goal of this study is to efficiently equip self-explaining models with visual explainability to address such computational challenges. To this end, we focus on *task arithmetic* [12], which enables model editing using *task vectors* that represent the model’s capabilities learned for different tasks across different domains. Interestingly, task vectors can represent *task analogies* expressed as “A is to B as C is to D,” where A and B are tasks in one domain (source domain), and C and D are tasks in another domain (target domain). If this analogy holds, the task vector for D can be inferred from those for A, B, and C, even if the model parameters for D are not available. This indicates that we can obtain the model parameters for task D without additional training of the model on that task.

Inspired by the idea, we propose a method to transfer the visual explainability of self-explaining models learned in a source domain to a target domain with task arithmetic. Our self-explaining model is an extension of image classifiers based on vision-language models, such as the Contrastive Language-Image Pretraining (CLIP) [13], which are designed to infer patch-level attributions from patch embeddings and the text embeddings of class labels, as well as to predict the logits of class labels similarly to the original vision-language models. Our model is trained on labeled image datasets with and without explanation supervision in the source domain. The difference between these two types of learned model parameters constitutes the task vector for explainability, which we refer to as the *explainability vector*. Based on the analogy for explainability: “prediction-only is to prediction-with-explanation in the source domain as prediction-only is to prediction-with-explanation in the target domain,” we provide a method to transfer explainability to a model that has been trained only for prediction in the target domain, by leveraging the explainability vector acquired in the source domain.

In the first experiment on 56 pairs of image classification datasets, we demonstrate that, except for transfers between some less-related domains, visual explainability can be successfully transferred from source to target domains, improving explanation quality in the target domain without sacrificing classification accuracy. We also show that the similarity of task vectors acquired from prediction-only tasks in source and target domains is moderately correlated with explanation quality. This suggests that the similarity could be a hint for predicting the success of explainability transfer. The second experiment shows that visual explainability learned on a large and diverse dataset like ImageNet [14] exhibits universality and robustness, improving explanation quality on nine out of ten different target datasets. The improvements of the explanations were qualitatively confirmed by comparing the ground-truth and predicted patch-level attributions. Additionally, we found that the explanation quality achieved with our model is comparable to that of Kernel SHAP on average, in which 150 model inferences are used.

Our contributions can be summarized as follows:

- We are the first to propose a method for transferring visual explainability from source to target domains with task arithmetic.
- Through the experiment on 56 pairs of image classification datasets, we found that the explainability transfer succeeds without sacrificing classification accuracy for many pairs of related domains.
- We constructed ImageNet+X, which extends ImageNet-1k to include explanation supervision generated using Kernel SHAP, and found that the explainability vector learned on ImageNet+X can improve explanation quality on various target domains.

2 Related Work

2.1 Task Arithmetic

Model merging is a technique for integrating multiple trained neural network models into a single model. Approaches to model merging include ensemble [15, 16], weight aggregation [17, 12, 18], and neuron alignment [19, 20]. Task arithmetic [12] is a type of the weight aggregation approach. A key feature of task arithmetic is that it allows for the composition or removal of skills that models have acquired through learning, without requiring additional training. Leveraging this, studies on model editing have explored topics such as adding mathematical reasoning capabilities [21], unlearning [22], mitigating bias [23], and reducing toxicity [12]. On the other hand, capability of task arithmetic for transferring visual explainability is unexplored.

Various studies have developed methods to improve the efficiency of task arithmetic techniques [24–28]. While this paper uses an original task arithmetic procedure [12] to focus on verifying the transferability of explainability, applying these efficiency-enhancing methods could lead to more effective explainability transfer.

2.2 Self-Explaining Vision Models

To improve the faithfulness and computational efficiency of explanations, various self-explaining models that are capable of performing both prediction and explanation have been proposed [29, 30, 9]. A pioneering work in self-explaining models for computer vision is the Class Activation Map (CAM) [31], which modifies the architecture of convolutional neural networks by introducing global average pooling before the fully connected layer, enabling both prediction and explanation based on weighted activation maps. In our model, which employs the Vision Transformer (ViT) [32] architecture, the attention map between the class token and image patches can be visualized to explain the importance of each image patch, indicating that the ViT architecture inherently possesses self-explaining characteristics. However, some studies have raised concerns about the validity of attention as an explanation [33–35]. For such concerns, several studies have proposed methods for training models with constraints that explicitly encourage attention to be more aligned with human-interpretable explanations [36–38].

As with our study, several studies have also addressed training self-explaining models to directly produce Shapley value-based explanations [11, 39]. These approaches guarantee that the explanations approximate Shapley values through the design of the objective function or network architecture, without requiring precomputed ground-truth Shapley value explanations. Similar approaches have been proposed in the research on amortized explainers [40], which learn the behavior of post-hoc explainers for a trained prediction model in advance and generate only explanations efficiently in the inference phase. Similar to ours, Covert et al. proposed a method that trains a ViT to output patch-level attributions based on Shapley values from patch tokens [41]. While this approach can efficiently train models to produce Shapley value explanations, it is difficult to generalize it to explanations other than Shapley values due to its specialization.

2.3 Visual Explainability Transfer

Some studies have proposed methods for transferring visual explainability to other domains. Transferrable Vision Explainer (TVE) [42] pretrains an encoder on a large-scale dataset like ImageNet to output meta-attribute vectors from images. In the inference phase, it uses a combination of this encoder and a pretrained classification head for the target task to output patch contributions. Although TVE is an amortized explainer and thus addresses a different problem than our method for self-explaining models, its objective of transferring pretrained explainability is consistent with the spirit of this study. Li et al. [43] demonstrated that transferring attention patterns from teacher to student models in ViT enables the student to achieve performance comparable to that of the teacher. Since attention patterns are often interpreted as explanations for model predictions, this method can be regarded as a form of explainability transfer. However, their results showed that such transfer is ineffective when the student and teacher models are trained on different domains.

3 Task Arithmetic

Before describing the proposed method, we first introduce the task arithmetic framework [12], which serves as the foundation for our approach. Task arithmetic edits neural network models by leveraging differences in their parameter spaces. The central idea is that the effect of learning a specific capability (or task) can be represented as a vector in the parameter space, and these vectors for different tasks can be algebraically combined to transfer or compose capabilities across models. The validity of task arithmetic is supported by the observations that aggregating models by adding multiple model parameters can improve model performance [44–46, 17, 47].

Formally, let $\theta_{\text{base}} \in \mathbb{R}^D$ denote the parameters of a base model where D is the dimensionality of the model parameters, and let $\theta_{\text{ft}} \in \mathbb{R}^D$ denote the parameters of the same model after fine-tuning on a specific task from the base parameters θ_{base} . The difference $\tau = \theta_{\text{ft}} - \theta_{\text{base}}$ is called the *task vector* for that task, which hopefully contains the knowledge and capabilities necessary to perform the task. The addition operation of task vectors allows us to construct a model that is capable of performing multiple tasks simultaneously, similar to multi-task learning. Specifically, given multiple task vectors $\{\tau_m\}_{m=1}^M$, where m is a task index, a new model composed of capabilities from these tasks can be constructed as

$$\theta = \theta_{\text{base}} + \lambda \sum_{m=1}^M \tau_m, \quad (1)$$

where $\lambda \in \mathbb{R}$ is a scaling factor controlling the extent to which the capabilities are added (if $\lambda > 0$) or removed (if $\lambda < 0$).

For a more complicated arithmetic operation that we are interested in, analogical relationships between tasks can be considered. Suppose we have models finetuned for tasks A and B in the same domain (referred to as *source domain* for

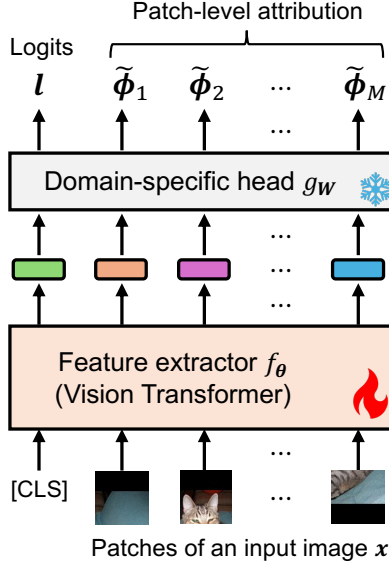


Figure 1: Model architecture. All the learnable parameters are only in the feature extractor.

convenience), and for task C in another domain (referred to as *target domain* for convenience). Our aim is to obtain model parameters θ that achieve a new task D. If the relationship between A and B is analogous to that between C and D, we can estimate the parameters for task D using the following analogy:

$$\tau_A - \tau_B = \tau_C - \tau_D \quad \rightarrow \quad \tau_D = \tau_C - \tau_A + \tau_B. \quad (2)$$

Then, we can endow the model with the capability for task D by adding the task vector τ_D to the base parameters θ_{base} as follows:

$$\theta = \theta_{\text{base}} + \lambda \tau_D. \quad (3)$$

This property enables us to transfer learned capabilities from a source domain to a target domain, even when direct supervision in the target domain (for task D in (2)) is unavailable. In the next section, we describe how we leverage task arithmetic to transfer the visual explainability of self-explaining models from the source to the target domains.

4 Proposed Method

This section describes the proposed method, which transfers visual explainability learned on a source domain to that for a target domain with task arithmetic.

4.1 Model

The proposed method requires a self-explaining image classifier (model) that predicts both the logits of class labels and infers patch-level attributions corresponding to the contributions of the patches for each class. As a requirement for the model to utilize task arithmetic, it is necessary that the model is represented by parameters $\theta \in \mathbb{R}^D$ even if the source and target label sets are different. In other words, the model should be capable of zero-shot classification. To satisfy the requirement, our self-explaining image classifier is designed as shown in Figure 1, which is an extension of the CLIP image classifier [13]. More specifically, our model consists of a feature extractor and a domain-specific head. We denote the input space as \mathcal{X} , and the number of patches in an input image as M . The feature extractor f_θ is a neural network with the Vision Transformer (ViT) architecture [48]. It takes M patches of an input image $x \in \mathcal{X}$ and a special token [CLS] as input and outputs $M + 1$ K -dimensional feature vectors. The domain-specific head is a linear function $g_W : \mathbb{R}^K \rightarrow \mathbb{R}^C$ with weights $W \in \mathbb{R}^{K \times C}$ where C is the number of classes. The function g_W maps the feature vector for [CLS] to logits $l = [l_1, l_2, \dots, l_C]^\top \in \mathbb{R}^C$ and that for the m th patch to patch-level attributions $\tilde{\phi}_m = [\tilde{\phi}_{m1}, \tilde{\phi}_{m2}, \dots, \tilde{\phi}_{mC}]^\top \in \mathbb{R}^C$, respectively, where $m \in \{1, 2, \dots, M\}$ is a patch index. We denote all the patch-level attributions as $\tilde{\Phi} = [\tilde{\phi}_1, \tilde{\phi}_2, \dots, \tilde{\phi}_M] \in \mathbb{R}^{C \times M}$. As with the original CLIP image classifiers, W is

constructed by the text embeddings representing the class names generated by the CLIP text encoder¹, i.e., $\mathbf{W}_{\cdot,c} \in \mathbb{R}^K$ is the text embedding associated with the c th class. In our model, \mathbf{W} is fixed during training; therefore, it is not included in the model parameters. The key difference from the original CLIP image classifier is that the domain-specific head is used for predicting not only the logits but also patch-level attributions, while the original CLIP image classifiers only predict the logits.

Our model can reuse the pretrained parameters of the original CLIP image classifiers as the base parameters θ_{base} . Note that they do not have the capability to explain the classification results because CLIP is not optimized for explanation.

4.2 Learning Classification Capability and Explainability

We acquire explainability on a source domain by finetuning our self-explaining image classifier in a supervised manner. First, we construct a source dataset, a labeled image dataset with explanation supervision $\mathcal{D}^S = \{(\mathbf{x}^{(n)}, y^{(n)}, \phi^{(n)})\}_{n=1}^{N^S}$ where $\mathbf{x}^{(n)} \in \mathcal{X}$ is the n th input image, $y^{(n)} \in \{1, 2, \dots, C^S\}$ is the ground-truth class label of the input $\mathbf{x}^{(n)}$, and $\phi^{(n)} \in \mathbb{R}^M$ is the ground-truth patch-level attributions given $\mathbf{x}^{(n)}$ and $y^{(n)}$. We can design the ground-truth patch-level attributions flexibly along user’s purposes and applications; they are typically given by human annotators or by computing a post-hoc explanation method, such as SHAP [6, 49] and Grad-CAM [7]. Since obtaining such attributions may be highly expensive, we assume that they are only available in the source domain.

Initialized at the base parameters θ_{base} , we learn the model parameters by solving the following optimization problem:

$$\theta_{\text{ft}\star}^S = \arg \min_{\theta} \mathcal{L}_{\alpha}(\theta; \mathcal{D}^S), \quad \text{where} \quad \mathcal{L}_{\alpha}(\theta; \mathcal{D}^S) = \alpha \mathcal{L}_{\text{cls}}(\theta; \mathcal{D}^S) + (1 - \alpha) \mathcal{L}_{\text{exp}}(\theta; \mathcal{D}^S), \quad (4)$$

where \mathcal{L}_{cls} is the cross-entropy loss between the logits and the ground-truth class label. The explanation loss \mathcal{L}_{exp} is defined as

$$\mathcal{L}_{\text{exp}}(\theta; \mathcal{D}^S) = \frac{1}{|\mathcal{D}^S|} \sum_{n=1}^{|\mathcal{D}^S|} \|\tilde{\Phi}_{y^{(n)}} - \phi^{(n)}\|_2^2, \quad (5)$$

where $\tilde{\Phi}_{y^{(n)}}$ is the $y^{(n)}$ th column of $\tilde{\Phi}$, which is the predicted patch-level attributions for the input $\mathbf{x}^{(n)}$ when it is classified as the $y^{(n)}$ th class. The hyperparameter $\alpha \in [0, 1]$ balances the two losses, \mathcal{L}_{cls} and \mathcal{L}_{exp} . When $\alpha = 1$, the learned parameters are identical to the finetuned parameters of the original CLIP image classifier, θ_{ft}^S , where the subscript ‘ft’ stands for finetuned only for classification. The case of $\alpha = 0$ results in amortized explainer [41, 50] where the learned parameters have only the explanatory capability. What we want are the model parameters $\theta_{\text{ft}\star}^S$ learned with $0 < \alpha < 1$ that have both the classification capability (denoted by ‘ft’) and the explainability (denoted by ‘ \star ’) in the source domain.

4.3 Transferring Visual Explainability

For the target domain, we assume that the ground-truth patch-level attributions are not available. In other words, while we cannot access the model parameters $\theta_{\text{ft}\star}^T$ that have both the classification capability and the explainability in the target domain, the model parameters θ_{ft}^T , which have only the classification capability, can be obtained by optimizing $\mathcal{L}_{\text{cls}}(\theta; \mathcal{D}^T)$, where \mathcal{D}^T is the labeled image dataset for the target domain without explanation supervision. Our goal is to transfer the explainability on the source domain included in $\theta_{\text{ft}\star}^S$ to θ_{ft}^T without additional training. That is, we aim at obtaining the model parameters $\tilde{\theta}_{\text{ft}\star}^T$, good approximation of $\theta_{\text{ft}\star}^T$, that have both the classification capability and the explainability for the target domain without the ground-truth patch-level attributions for the target domain.

To this end, we utilize the task arithmetic framework introduced in Section 3. Based on the task analogy (2), the task vectors obtained from the parameters trained on the source and target domains are expected to have the following relationship:

$$\tau_{\text{ft}\star}^S - \tau_{\text{ft}}^S = \tau_{\text{ft}\star}^T - \tau_{\text{ft}}^T, \quad (6)$$

where $\tau_{\text{ft}\star}^S = \theta_{\text{ft}\star}^S - \theta_{\text{base}}$ and $\tau_{\text{ft}\star}^T = \theta_{\text{ft}\star}^T - \theta_{\text{base}}$ are the task vectors representing both the classification capability and explainability for the source and target domains, respectively. $\tau_{\text{ft}}^S = \theta_{\text{ft}}^S - \theta_{\text{base}}$ and $\tau_{\text{ft}}^T = \theta_{\text{ft}}^T - \theta_{\text{base}}$ are the task vectors representing only the classification capability for the source and target domains, respectively. The equality holds if and only if $\tau_{\star}^S = \tau_{\star}^T$, where $\tau_{\star}^S = \theta_{\text{ft}\star}^S - \theta_{\text{ft}}^S$ and $\tau_{\star}^T = \theta_{\text{ft}\star}^T - \theta_{\text{ft}}^T$ are the task vectors representing the explainability

¹For example, if the class name is ‘‘cat,’’ we use the mean of text embeddings generated by using the text encoder for multiple input texts, such as ‘‘a photo of cat’’, ‘‘art of the cat’’, ‘‘an origami cat’’, and so on.

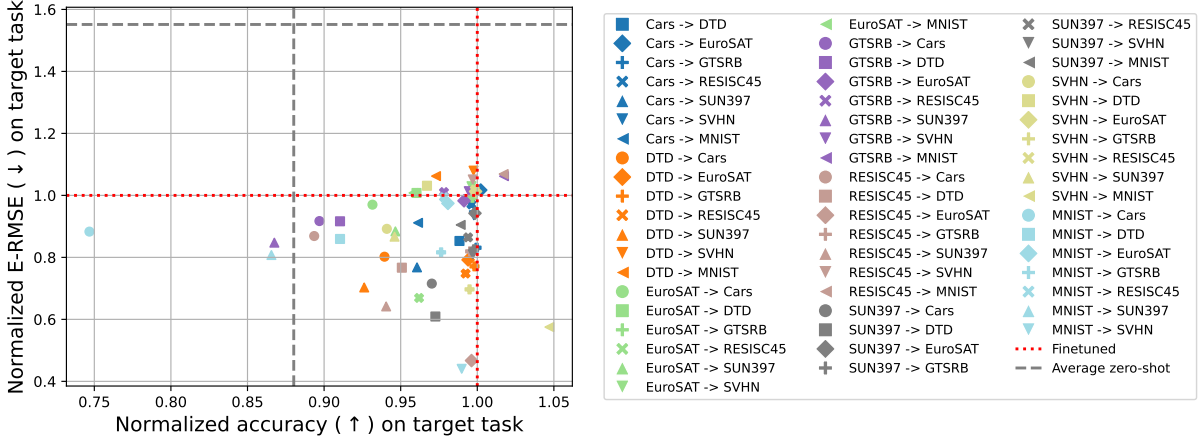


Figure 2: Normalized accuracies (larger is better) and normalized E-RMSEs (lower is better) in all the pairs of the eight benchmark datasets when fixed in $\alpha = 0.5$ and $\lambda_2 = 0.8$. The color and shape of each marker indicate the source and target domains of the corresponding dataset pair, respectively.

for the source and target domains, respectively. We refer to τ_*^S and τ_*^T as *explainability vectors* for the source and target domains, respectively.

From (6), τ_{ft*}^T can be expressed as

$$\tau_{ft*}^T = \underbrace{\theta_{ft}^T - \theta_{base}}_{\tau_{ft}^T} + \underbrace{\theta_{ft*}^S - \theta_{base}}_{\tau_{ft*}^S} - \underbrace{(\theta_{ft}^S - \theta_{base})}_{\tau_{ft}^S} = \underbrace{\theta_{ft}^T - \theta_{base}}_{\tau_{ft}^T} + \underbrace{\theta_{ft*}^S - \theta_{ft}^S}_{\tau_*^S}. \quad (7)$$

Then, we can obtain the model parameters $\tilde{\theta}_{ft*}^T$ by adding the task vector τ_{ft*}^T calculated in (7) to the base parameters θ_{base} . Specifically, we introduce two scaling coefficient hyperparameters, $\lambda_1 \in \mathbb{R}$ and $\lambda_2 \in \mathbb{R}$, and calculate them using the following equation:

$$\tilde{\theta}_{ft*}^T = \theta_{base} + \lambda_1 \tau_{ft}^T + \lambda_2 \tau_*^S. \quad (8)$$

Here, since λ_1 and λ_2 do not appear in the model training, which is a computationally expensive phase, these hyperparameters can be tuned efficiently.

Evaluating $\tau_*^S = \tau_*^T$. Accurately evaluating whether τ_*^S equals τ_*^T plays a crucial role in validating the effectiveness of our approach. The extent to which $\tau_*^S = \tau_*^T$ holds is quantified by the cosine similarity of τ_*^S and τ_*^T . Although τ_*^T is unknown, the similarity of τ_*^S and τ_*^T can be approximated with the similarity of τ_{ft*}^S and τ_{ft}^T empirically. The validity of the approximation is supported by the observation that the similarity of τ_*^S and τ_*^T is significantly correlated with that of τ_{ft*}^S and τ_{ft}^T (Pearson’s $r = 0.90$, $p < 0.01$), as shown in Figure 3(b).

5 Experiments

We conducted experiments on various image classification datasets to evaluate the effectiveness of the proposed method in explainability transfer.

Throughout our experiments, we used CLIP with ViT-B/32 [48] as the self-explaining image classifier, and its base parameters θ_{base} were the pre-trained parameters learned on DataComp-1B [51, 52]. The model input is a 224×224 RGB image, each patch size of an image is 32×32 , and the number of patches in an image is $M = 49$. The hyperparameter λ_1 was set to 1.0 to focus on investigating the effect of transferring explainability via τ_*^S while preserving high classification performance on target domains. The remaining hyperparameters, α and λ_2 , were determined within the range of $\{0.1, 0.2, \dots, 0.9\}$ and $\{0.0, 0.1, \dots, 1.2\}$, respectively, unless otherwise specified.

5.1 Transferring Explainability Between Various Domain Datasets

In our first experiment, we used eight labeled image datasets: Cars [53], DTD [54], EuroSAT [55], GTSRB [56], RESISC45 [57], SUN397 [58], SVHN [59], and MNIST [60]. We extended each of these datasets to include ground-

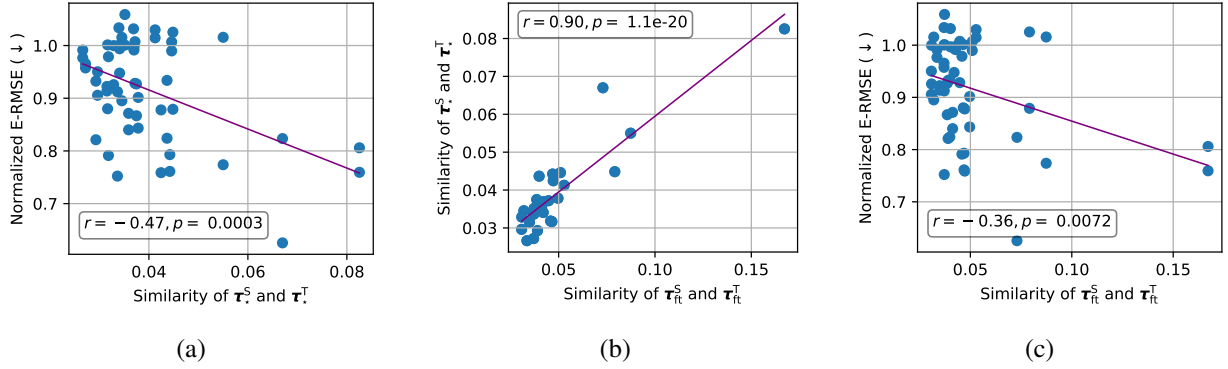


Figure 3: Relationships between two values for each dataset pair indicated in a blue point: (a) the similarity of τ_*^S and τ_*^T and E-RMSE, (b) the similarity of τ_*^S and τ_*^T and that of τ_{ft}^S and τ_{ft}^T , and (c) the similarity of τ_{ft}^S and τ_{ft}^T and E-RMSE. The purple solid line shows the least-squares regression fitted to the blue points, and the Pearson’s correlation coefficient r and its p -value are reported in the box of each panel.

truth patch-level attributions generated using Kernel SHAP [6, 49], which explain the classification results of the CLIP image classifier finetuned on each dataset. Here, the number of perturbations for each image in Kernel SHAP is set to 500. Similar methods for generating explanation supervision have been used in previous studies [50, 61]. We created 56 dataset pairs from the eight datasets, where one dataset in each pair was used as the source dataset, and the other as the target dataset.

In the proposed method, we first learned the three types of model parameters θ_{ft}^S , θ_{ft*}^S , and θ_{ft}^T for each dataset pair, and then obtained the model parameters $\tilde{\theta}_{ft*}^T$ by applying the proposed explainability transfer (8). We evaluated the quality of $\tilde{\theta}_{ft*}^T$ by the classification accuracy and the explanation error using explanation root mean squared error (E-RMSE), which is defined as $\sqrt{\mathcal{L}_{exp}(\theta; \mathcal{D}^T)}$ where \mathcal{D}^T is the target dataset with explanation supervision.

Accuracy and Explanation Error Trade-off. The first result, illustrated in Figure 2, shows the normalized accuracies and the normalized E-RMSEs for all the dataset pairs. Here, the normalized scores are obtained by dividing the corresponding scores of θ_{ft}^T , which are finetuned on the target dataset without explanation supervision. The red dotted line indicates the performances of θ_{ft}^T (both the accuracy and E-RMSE are one), while the gray dashed line indicates those of the zero-shot classifier parameterized by θ_{base} . In successful cases, the E-RMSE values are decreased from one while keeping the accuracy close to one. From the figure, we found the decreases of the E-RMSEs for many of the dataset pairs while keeping 90% of the accuracy. In particular, we observed that transferring between datasets within the same domain, such as the pair of MNIST and SVHN or the pair of RESISC45 and EuroSAT, successfully maintains explainability while preserving classification accuracy. On the other hand, when transferring from MNIST to Cars, the accuracy dropped significantly. Similarly, when transferring from natural image domains (e.g., DTD and RESISC45) to text recognition image domains (e.g., MNIST and SVHN), the E-RMSEs deteriorated.

Impact of Similarity of Explainability Vectors. The task analogy (6) strictly holds if and only if $\tau_*^S = \tau_*^T$. In practice, the difference of the norms between τ_*^S and τ_*^T does not affect the performance because we take τ_*^S into account with the scalar multiplication by λ_2 as in (8). Thus, we evaluated the extent to which this condition holds using the cosine similarity of the explainability vectors τ_*^S and τ_*^T , which focuses on evaluating the alignment of the vectors’ directions rather than their scaling. Assessing the relationship between the performance of explainability transfer and the similarity of τ_*^S and τ_*^T is an important task to bridge the theory and the experimental result. Figure 3(a) shows the relationship between the similarity of τ_*^S and τ_*^T and the E-RMSE for each dataset pair, and we observed a statistically significant negative correlation between the similarity of the explainability vectors and the E-RMSE (Pearson’s $r = -0.47$, $p < 0.01$). This result indicates that a higher similarity between explainability vectors could lead to a lower E-RMSE, indicating better explainability transfer.

Since the similarity of τ_*^S and τ_*^T cannot be directly evaluated due to the unknown τ_*^T , we approximated it using the similarity of τ_{ft}^S and τ_{ft}^T , which can be computed without explanation supervision. Figure 3(b) shows the relationship between the two similarities, and we found a statistically significant and strongly positive correlation between them (Pearson’s $r = 0.90$, $p < 0.01$).

Table 1: Average performances over the ten target datasets when transferring explainability learned on ImageNet+X. **Bold and underlined values** indicate the best for each metric, while **bold values** indicate that there is no statistically significant difference from the best, as determined by a t -test ($p < 0.05$).

Model	Param.	Accuracy (\uparrow)	E-RMSE (\downarrow)	IoU@1 (\uparrow)	IoU@10 (\uparrow)	Infidelity (\downarrow)
Zero-shot	θ_{base}	0.475 ± 0.211	1.313 ± 0.225	0.012 ± 0.006	0.090 ± 0.021	2.421 ± 0.834
Finetuned on ImageNet	$\theta_{\text{ft}}^{\text{S}}$	0.363 ± 0.242	1.179 ± 0.136	0.008 ± 0.007	0.072 ± 0.028	1.892 ± 0.453
Finetuned on ImageNet+X	$\theta_{\text{ft},*}^{\text{S}}$	0.367 ± 0.238	<u>0.907 ± 0.155</u>	<u>0.041 ± 0.013</u>	<u>0.147 ± 0.033</u>	<u>1.130 ± 0.345</u>
Finetuned on target	$\theta_{\text{ft}}^{\text{T}}$	<u>0.890 ± 0.106</u>	1.599 ± 0.219	0.009 ± 0.005	0.076 ± 0.021	3.535 ± 0.978
Proposed	$\tilde{\theta}_{\text{ft},*}^{\text{T}}$	<u>0.876 ± 0.121</u>	<u>0.943 ± 0.186</u>	<u>0.071 ± 0.082</u>	<u>0.166 ± 0.052</u>	<u>1.228 ± 0.394</u>

Building on these results, we investigated whether the similarity of $\tau_{\text{ft}}^{\text{S}}$ and $\tau_{\text{ft}}^{\text{T}}$ could serve as a predictor for the success of explainability transfer. Figure 3(c) shows the relationship between the similarity of $\tau_{\text{ft}}^{\text{S}}$ and $\tau_{\text{ft}}^{\text{T}}$ and the E-RMSE for each dataset pair, and we found a statistically significant negative correlation between them (Pearson’s $r = -0.36$, $p < 0.01$). Although a significant correlation was observed, it is important to note that the correlation was weaker than that between the similarity of τ_{*}^{S} and τ_{*}^{T} and the E-RMSE. This suggests that we should utilize the similarity of $\tau_{\text{ft}}^{\text{S}}$ and $\tau_{\text{ft}}^{\text{T}}$ carefully for predicting the success of explainability transfer.

5.2 Transferring Explainability Learned on ImageNet

In the previous section, we showed that explainability can be transferred from source to target domains such that the task vectors $\tau_{\text{ft}}^{\text{S}}$ and $\tau_{\text{ft}}^{\text{T}}$ are similar. However, the datasets used in the previous section have limited coverage on the source domain. This fact may restrict the performance of explainability transfer. Conversely, the fact raises the intriguing possibility that explainability learned on a larger and more diverse dataset, such as ImageNet, could serve as a universal explainability vector, transferable across a wide range of domains. To explore the potential, we verify whether we can transfer explainability learned on ImageNet to other datasets.

To learn explainability on ImageNet, we constructed the ImageNet+X dataset. In the ImageNet+X dataset, every sample consists of a labeled image from the original ImageNet-1k dataset and a ground-truth patch-level attribution generated as with the previous section. As the target datasets, we used 10 image classification datasets, which include the eight datasets used in the previous section and two additional datasets: CIFAR100 [62] and STL10 [63]. As with ImageNet+X, we added the ground-truth patch-level attributions to the 10 datasets.

In addition to classification accuracies and E-RMSEs, we also evaluated the explanation qualities using IoU@1, IoU@10 [64, 65], and infidelity [66]. IoU@ K ($K \in \{1, 10\}$) is the intersection over union (IoU) between the predicted patch-level attributions and the ground-truth ones, which is calculated as the degree of overlap between the indices of the top- K predicted patch-level attributions and those of the top- K ground-truth ones. IoU@ K is useful for evaluating the correctness of highlighted patches. Infidelity measures how accurately an explanation reflects the behavior of a classifier by quantifying the discrepancy between the attributions assigned to patches and the actual changes in model output when those patches are perturbed.

Quantitative Results. Table 1 shows the average performances of the explainability transferred by the proposed method, in comparison to the models with the parameters θ_{base} , $\theta_{\text{ft}}^{\text{S}}$, $\theta_{\text{ft},*}^{\text{S}}$, and $\theta_{\text{ft}}^{\text{T}}$. The highest accuracy was achieved by the model finetuned on the target dataset without explanation supervision, i.e., $\theta_{\text{ft}}^{\text{T}}$. Nevertheless, this model had the worst or second-worst explanation performance, indicating a lack of explainability. In contrast, the best E-RMSE and infidelity scores were achieved by the model finetuned on ImageNet+X, $\theta_{\text{ft},*}^{\text{S}}$, but this model had the second-lowest accuracy, indicating insufficient classification capability. Notably, the proposed method achieved a balance between high accuracy and strong explainability, with performance comparable to the best models in both respects. This indicates that the proposed method effectively transfers explainability while preserving classification capability, and that the explainability learned on ImageNet+X serves as a robust and generalizable explainability vector applicable across diverse datasets.

Impact of Scaling Coefficient. In Figure 4, we show the normalized E-RMSE, IoU@10, and accuracy for each target dataset over the scaling coefficient $\lambda_2 \in \{0.0, 0.1, \dots, 1.2\}$. As shown in Figure 4(a) and (b), although there are variations across datasets, increasing λ_2 generally improves the explanation scores. Larger λ_2 can lead to better explainability, but may also result in a drop in classification accuracy on the target domain because the most accurate

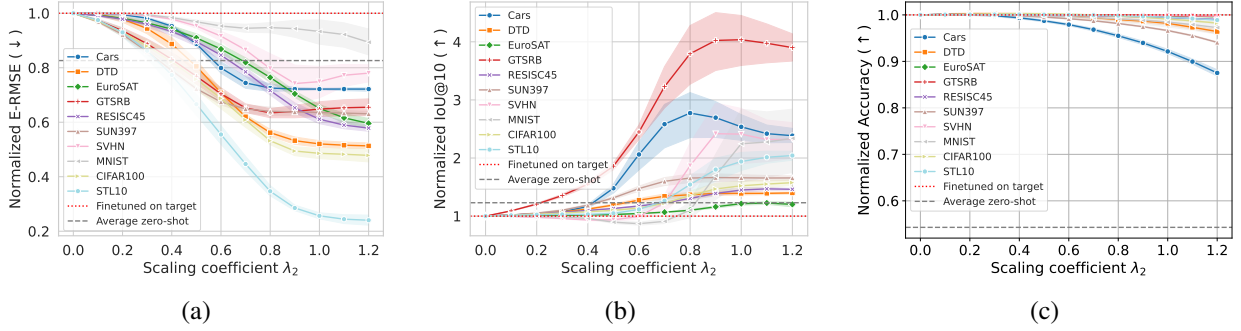


Figure 4: Normalized (a) E-RMSE, (b) IoU@10, and (c) accuracy for each target dataset over the scaling coefficients λ_2 . The shaded areas represent 95% confidence intervals of the performance for $\alpha \in \{0.1, 0.2, \dots, 0.9\}$.

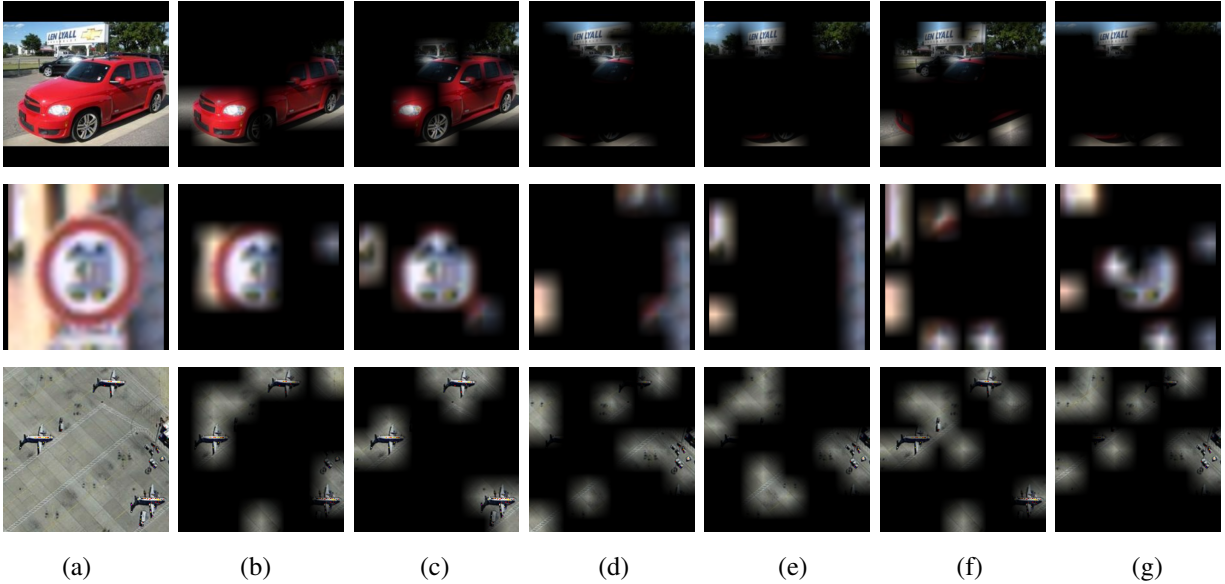


Figure 5: Visualization examples highlighting the top-10 patches in the predicted patch-level attributions. Rows show (from top to bottom) the results for Cars, GTSRB, and RESISC45 datasets, and columns show (from left to right) (a) input image, (b) ground-truth, (c) the proposed method, (d) finetuned on target dataset, (e) finetuned on ImageNet, (f) finetuned on ImageNet+X, and (g) zero-shot.

model $\theta_{\text{ft}}^{\text{T}}$ is modified by $\lambda\tau_{*}^{\text{S}}$. In Figure 4(c), we found that the accuracy tends to decrease as λ_2 increases; however, the accuracy is still above 90% for $\lambda_2 \leq 1.0$.

It is particularly noteworthy that the IoU@10 scores improved even though our objective does not directly optimize them. IoU@10 evaluates the correctness of the positions of important pixels. In applications where the goal is to highlight important regions of an image, achieving a higher IoU@10 is more important than minimizing E-RMSE. In the following experimental results, we focus on evaluating explanation quality in the perspective of IoU@10.

Qualitative Evaluation. To evaluate the predicted patch-level attributions qualitatively, we visualized the top-10 patches in the attributions produced by the proposed method and the other methods in Figure 5. Here, this visualization method aligns with the evaluation of IoU@10. As shown in the figure, the patches highlighted by the proposed method (depicted in Figure 5(c)) were more similar to the ground-truth ones (depicted in Figure 5(b)) than those predicted by the other methods. In the third row, the finetuned model on ImageNet+X (depicted in Figure 5(f)) also showed a good result because the proposed method transfers the explainability learned on ImageNet+X. It is worth mentioning that while the finetuned model on ImageNet+X demonstrates improved explainability, its classification accuracy on the target dataset is low. Consequently, the visualized results may not fully reflect the model’s performance in real-world scenarios where ground-truth labels are unavailable.

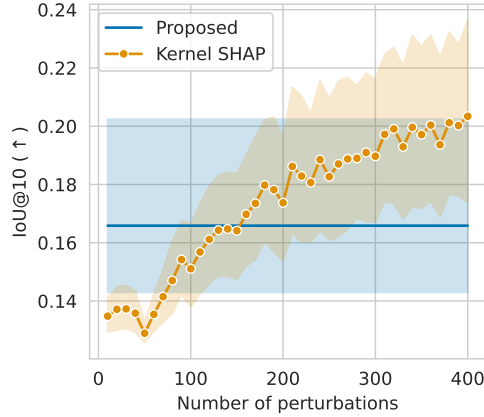


Figure 6: IoU@10 scores of the proposed method and Kernel SHAP averaged across the target datasets with varying number of perturbations. The shaded area represents the 95% confidence interval.

Comparison with Kernel SHAP. In our experiments, we used Kernel SHAP to generate the ground-truth patch-level attributions. Kernel SHAP requires classification results for multiple perturbations of the input image to compute patch-level attributions, which can be computationally expensive. Our self-explaining image classifier is designed to predict these attributions accurately in a single inference. How many perturbations are required for Kernel SHAP to achieve explanation quality comparable to that of our model? Figure 6 shows the IoU@10 scores averaged across all the target datasets as the number of perturbations used in Kernel SHAP increases. The results indicate that, on average, 150 perturbations are needed for Kernel SHAP to achieve IoU@10 scores equivalent to those of the proposed model. In other words, the proposed model successfully achieves explanation quality comparable to Kernel SHAP with only 1/150 of the inference cost, significantly reducing the computational expense of generating explanations.

The difference between our “prediction-with-explanation” model and the “prediction-only” model used by Kernel SHAP is that the former applies the domain-specific head g_W to both the [CLS] token and the M image patches, while the latter applies it only to the [CLS] token. Regarding the computational complexity of the feature extractor f_θ as a constant, the computational complexity of our model per explanation is $\mathcal{O}(M)$ where M is the number of patches in an image. In contrast, the computational complexity of Kernel SHAP per explanation is $\mathcal{O}(P + PM^2)$, where P is the number of perturbations and PM^2 is associated with solving the least-squares problem. The computational complexity of Kernel SHAP increases linearly with the number of perturbations P and quadratically with the number of patches M , suggesting that the complexity increases as the number of perturbations increases to improve explanation quality and as the model size increases to improve predictive performance. On the other hand, our model’s complexity increases linearly only with the number of patches M (i.e., the model size) and is independent of the explainability transfer procedure.

6 Conclusion

In this study, we proposed a method for transferring visual explainability of self-explaining models learned on labeled image datasets with explanation supervision through task arithmetic. Since our self-explaining models are straightforward extensions of zero-shot image classifiers based on vision-language pretrained models such as CLIP, the acquired explainability can be transferred to existing finetuned image classifiers specialized in prediction without additional training. In the experiments, we validated the transfer of explainability between pairs of datasets with limited domain coverage, and demonstrated that the transfer of explainability is successful between related domains. Additionally, we constructed ImageNet+X, an extended version of ImageNet that includes explanation supervision obtained using Kernel SHAP, and verified whether the explainability learned on ImageNet+X can be transferred to other image classification datasets. The results showed that the proposed method can improve explanation quality in most datasets without sacrificing classification accuracy, indicating that the explainability learned on ImageNet+X serves as an explainability vector applicable to diverse domains. The explanation quality achieved with a single model inference using the proposed method is, on average, comparable to that of Kernel SHAP, which requires 150 model inferences, indicating that the proposed method can generate explanations significantly efficiently than Kernel SHAP.

The results of this study suggest that once explainability vectors capable of generating human-desired explanations are acquired, their own explainability can be imparted to finetuned image recognition models specialized in prediction

without additional training. However, we found that the explainability vectors learned on ImageNet+X do not always improve the quality of explanations in some domains. This may be due to insufficient domain coverage of ImageNet+X, the insufficient capacity of the model used in this study, or technical challenges in task arithmetic. Further research to address these challenges is needed to create universal explainability vectors that can improve explanation quality across a broader range of domains.

References

- [1] Sajid Nazir, Diane M Dickson, and Muhammad Usman Akram. Survey of explainable artificial intelligence techniques for biomedical imaging with deep neural networks. *Computers in Biology and Medicine*, 156:106668, 2023.
- [2] Shahin Atakishiyev, Mohammad Salameh, Hengshuai Yao, and Randy Goebel. Explainable artificial intelligence for autonomous driving: A comprehensive overview and field guide for future research directions. *IEEE Access*, 2024.
- [3] Zoe Alexander, Duen Horng Chau, and Christopher Saldaña. An interrogative survey of explainable ai in manufacturing. *IEEE Transactions on Industrial Informatics*, 2024.
- [4] Nicola Capuano, Giuseppe Fenza, Vincenzo Loia, and Claudio Stanzione. Explainable artificial intelligence in cybersecurity: A survey. *IEEE Access*, 10:93575–93600, 2022.
- [5] Andrea Apicella, Luca Di Lorenzo, Francesco Isgrò, Andrea Pollastro, and Roberto Prevete. Strategies to exploit xai to improve classification systems. In *World Conference on Explainable Artificial Intelligence*, pages 147–159. Springer, 2023.
- [6] Scott M Lundberg and Su-In Lee. A Unified Approach to Interpreting Model Predictions. *Advances in Neural Information Processing Systems*, pages 4765–4774, 2017.
- [7] Ramprasaath R Selvaraju, Michael Cogswell, Abhishek Das, Ramakrishna Vedantam, Devi Parikh, and Dhruv Batra. Grad-CAM: Visual Explanations from Deep Networks via Gradient-Based Localization. *International Journal of Computer Vision*, 128(2):336–359, 2020.
- [8] David Alvarez Melis and Tommi Jaakkola. Towards robust interpretability with self-explaining neural networks. *Advances in Neural Information Processing Systems*, 31, 2018.
- [9] Yang Ji, Ying Sun, Yuting Zhang, Zhigaoyuan Wang, Yuanxin Zhuang, Zheng Gong, Dazhong Shen, Chuan Qin, Hengshu Zhu, and Hui Xiong. A comprehensive survey on self-interpretable neural networks. *arXiv preprint arXiv:2501.15638*, 2025.
- [10] Andrew Slavin Ross, Michael C Hughes, and Finale Doshi-Velez. Right for the right reasons: Training differentiable models by constraining their explanations. In *Proceedings of the Twenty-Sixth International Joint Conference on Artificial Intelligence*, pages 2662–2670. International Joint Conferences on Artificial Intelligence Organization, 2017.
- [11] Rui Wang, Xiaoqian Wang, and David Inouye. Shapley explanation networks. In *International Conference on Learning Representations*, 2021.
- [12] Gabriel Ilharco, Marco Tulio Ribeiro, Mitchell Wortsman, Suchin Gururangan, Ludwig Schmidt, Hannaneh Hajishirzi, and Ali Farhadi. Editing models with task arithmetic. *arXiv preprint arXiv:2212.04089*, 2023.
- [13] Alec Radford, Jong Wook Kim, Chris Hallacy, Aditya Ramesh, Gabriel Goh, Sandhini Agarwal, Girish Sastry, Amanda Askell, Pamela Mishkin, Jack Clark, et al. Learning transferable visual models from natural language supervision. In *International Conference on Machine Learning (ICML)*, pages 8748–8763, 2021.
- [14] Jia Deng, Wei Dong, Richard Socher, Li-Jia Li, Kai Li, and Li Fei-Fei. Imagenet: A large-scale hierarchical image database. In *2009 IEEE conference on computer vision and pattern recognition*, pages 248–255. IEEE, 2009.
- [15] Gao Huang, Yixuan Li, Geoff Pleiss, Zhuang Liu, John E Hopcroft, and Kilian Q Weinberger. Snapshot ensembles: Train 1, get m for free. In *International Conference on Learning Representations*, 2017.
- [16] Noam Shazeer, Azalia Mirhoseini, Krzysztof Maziarz, Andy Davis, Quoc Le, Geoffrey Hinton, and Jeff Dean. Outrageously large neural networks: The sparsely-gated mixture-of-experts layer. In *International Conference on Learning Representations*, 2017.
- [17] Mitchell Wortsman, Gabriel Ilharco, Samir Ya Gadre, Rebecca Roelofs, Raphael Gontijo-Lopes, Ari S Morcos, Hongseok Namkoong, Ali Farhadi, Yair Carmon, Simon Kornblith, et al. Model soups: averaging weights of multiple fine-tuned models improves accuracy without increasing inference time. In *International conference on machine learning*, pages 23965–23998. PMLR, 2022.

- [18] G Stoica, D Bolya, J Bjorner, P Ramesh, T Hearn, and J Hoffman. Zipit! merging models from different tasks without training. In *International Conference on Learning Representations*. International Conference on Learning Representations, 2024.
- [19] Samuel K Ainsworth, Jonathan Hayase, and Siddhartha Srinivasa. Git re-basin: Merging models modulo permutation symmetries. *arXiv preprint arXiv:2209.04836*, 2022.
- [20] Sidak Pal Singh and Martin Jaggi. Model fusion via optimal transport. *Advances in Neural Information Processing Systems*, 33:22045–22055, 2020.
- [21] Shiqi Chen, Jinghan Zhang, Tongyao Zhu, Wei Liu, Siyang Gao, Miao Xiong, Manling Li, and Junxian He. Bring reason to vision: Understanding perception and reasoning through model merging. *arXiv preprint arXiv:2505.05464*, 2025.
- [22] Shiwen Ni, Dingwei Chen, Chengming Li, Xiping Hu, Ruifeng Xu, and Min Yang. Forgetting before learning: Utilizing parametric arithmetic for knowledge updating in large language models. In *Proceedings of the 62nd Annual Meeting of the Association for Computational Linguistics (Volume 1: Long Papers)*, pages 5716–5731, 2024.
- [23] Daiki Shirafuji, Makoto Takenaka, and Shinya Taguchi. Bias vector: Mitigating biases in language models with task arithmetic approach. In *Proceedings of the 31st International Conference on Computational Linguistics*, pages 2799–2813, 2025.
- [24] Michael S Matena and Colin A Raffel. Merging models with fisher-weighted averaging. *Advances in Neural Information Processing Systems*, 35:17703–17716, 2022.
- [25] Guillermo Ortiz-Jimenez, Alessandro Favero, and Pascal Frossard. Task arithmetic in the tangent space: Improved editing of pre-trained models. *Advances in Neural Information Processing Systems*, 36:66727–66754, 2023.
- [26] Prateek Yadav, Derek Tam, Leshem Choshen, Colin A Raffel, and Mohit Bansal. Ties-merging: Resolving interference when merging models. *Advances in Neural Information Processing Systems*, 36:7093–7115, 2023.
- [27] Le Yu, Bowen Yu, Haiyang Yu, Fei Huang, and Yongbin Li. Language models are super mario: Absorbing abilities from homologous models as a free lunch. In *Forty-first International Conference on Machine Learning*, 2024.
- [28] Kotaro Yoshida, Yuji Naraki, Takafumi Horie, Ryosuke Yamaki, Ryotaro Shimizu, Yuki Saito, Julian McAuley, and Hiroki Naganuma. Mastering task arithmetic: τ_{jp} as a key indicator for weight disentanglement. In *The Thirteenth International Conference on Learning Representations*, 2025.
- [29] Rami Ibrahim and M Omair Shafiq. Explainable convolutional neural networks: a taxonomy, review, and future directions. *ACM Computing Surveys*, 55(10):1–37, 2023.
- [30] Antonio Di Marino, Vincenzo Bevilacqua, Angelo Ciamarella, Ivanoe De Falco, and Giovanna Sannino. Ante-hoc methods for interpretable deep models: A survey. *ACM Computing Surveys*, 57(10):1–36, 2025.
- [31] Bolei Zhou, Aditya Khosla, Agata Lapedriza, Aude Oliva, and Antonio Torralba. Learning deep features for discriminative localization. In *Proceedings of the IEEE conference on computer vision and pattern recognition*, pages 2921–2929, 2016.
- [32] Alexey Dosovitskiy, Lucas Beyer, Alexander Kolesnikov, Dirk Weissenborn, Xiaohua Zhai, Thomas Unterthiner, Mostafa Dehghani, Matthias Minderer, G Heigold, S Gelly, et al. An image is worth 16x16 words: Transformers for image recognition at scale. In *International Conference on Learning Representations*, 2020.
- [33] Sofia Serrano and Noah A Smith. Is attention interpretable? In *Proceedings of the 57th Annual Meeting of the Association for Computational Linguistics*, pages 2931–2951, 2019.
- [34] Sarthak Jain and Byron C Wallace. Attention is not explanation. In *Proceedings of the 2019 Conference of the North American Chapter of the Association for Computational Linguistics: Human Language Technologies, Volume 1 (Long and Short Papers)*, pages 3543–3556, 2019.
- [35] Hila Chefer, Shir Gur, and Lior Wolf. Transformer interpretability beyond attention visualization. In *Proceedings of the IEEE/CVF Conference on Computer Vision and Pattern Recognition*, pages 782–791, 2021.
- [36] Lu Yu, Wei Xiang, Juan Fang, Yi-Ping Phoebe Chen, and Lianhua Chi. ex-vit: A novel explainable vision transformer for weakly supervised semantic segmentation. *Pattern Recognition*, 142:109666, 2023.
- [37] Yao Qiang, Chengyin Li, Prashant Khanduri, and Dongxiao Zhu. Interpretability-aware vision transformer. *arXiv preprint arXiv:2309.08035*, 2023.
- [38] Ananthu Aniraj, Cassio F. Dantas, Dino Ienco, and Diego Marcos. Inherently faithful attention maps for vision transformers, 2025. URL <https://arxiv.org/abs/2506.08915>.

- [39] Amr Alkhatib, Roman Bresson, Henrik Boström, and Michalis Vazirgiannis. Prediction via shapley value regression. *arXiv preprint arXiv:2505.04775*, 2025.
- [40] Yu-Neng Chuang, Guanchu Wang, Fan Yang, Zirui Liu, Xuanting Cai, Mengnan Du, and Xia Hu. Efficient xai techniques: A taxonomic survey. *arXiv preprint arXiv:2302.03225*, 2023.
- [41] Ian Connick Covert, Chanwoo Kim, and Su-In Lee. Learning to estimate shapley values with vision transformers. In *The Eleventh International Conference on Learning Representations*, 2023.
- [42] Guanchu Wang, Yu-Neng Chuang, Fan Yang, Mengnan Du, Chia-Yuan Chang, Shaochen Zhong, Zirui Liu, Zhaozhuo Xu, Kaixiong Zhou, Xuanting Cai, et al. Tve: Learning meta-attribution for transferable vision explainer. In *International Conference on Machine Learning*, pages 50248–50267. PMLR, 2024.
- [43] Alex Li, Yuandong Tian, Beidi Chen, Deepak Pathak, and Xinlei Chen. On the surprising effectiveness of attention transfer for vision transformers. *Advances in Neural Information Processing Systems*, 37:113963–113990, 2024.
- [44] P Izmailov, AG Wilson, D Podoprikin, D Vetrov, and T Garipov. Averaging weights leads to wider optima and better generalization. In *34th Conference on Uncertainty in Artificial Intelligence 2018, UAI 2018*, pages 876–885, 2018.
- [45] Arthur Jacot, Franck Gabriel, and Clément Hongler. Neural tangent kernel: Convergence and generalization in neural networks. *Advances in neural information processing systems*, 31, 2018.
- [46] Hiroki Naganuma, Kotaro Yoshida, Laura Gomezjurado Gonzalez, Takafumi Horie, Yuji Naraki, and Ryotaro Shimizu. On fairness of task arithmetic: The role of task vectors. *arXiv preprint arXiv:2505.24262*, 2025.
- [47] Mitchell Wortsman, Gabriel Ilharco, Jong Wook Kim, Mike Li, Simon Kornblith, Rebecca Roelofs, Raphael Gontijo Lopes, Hannaneh Hajishirzi, Ali Farhadi, Hongseok Namkoong, et al. Robust fine-tuning of zero-shot models. In *Proceedings of the IEEE/CVF conference on computer vision and pattern recognition*, pages 7959–7971, 2022.
- [48] Alexey Dosovitskiy, Lucas Beyer, Alexander Kolesnikov, Dirk Weissenborn, Xiaohua Zhai, Thomas Unterthiner, Mostafa Dehghani, Matthias Minderer, Georg Heigold, Sylvain Gelly, Jakob Uszkoreit, and Neil Houlsby. An image is worth 16x16 words: Transformers for image recognition at scale. In *International Conference on Learning Representations*, 2021. URL <https://openreview.net/forum?id=YicbFdNTTy>.
- [49] shap (Github). shap: A game theoretic approach to explain the output of any machine learning model, 2024. URL <https://github.com/shap/shap>. Accessed: 2024-2-2.
- [50] Chenghao Yang, Fan Yin, He He, Kai-Wei Chang, Xiaofei Ma, and Bing Xiang. Efficient shapley values estimation by amortization for text classification. In *Proceedings of the 61st Annual Meeting of the Association for Computational Linguistics (Volume 1: Long Papers)*, pages 8666–8680, 2023.
- [51] Samir Yitzhak Gadre, Gabriel Ilharco, Alex Fang, Jonathan Hayase, Georgios Smyrnis, Thao Nguyen, Ryan Marten, Mitchell Wortsman, Dhruva Ghosh, Jieyu Zhang, Eyal Orgad, Rahim Entezari, Giannis Daras, Sarah Pratt, Vivek Ramanujan, Yonatan Bitton, Kalyani Marathe, Stephen Mussmann, Richard Vencu, Mehdi Cherti, Ranjay Krishna, Pang Wei Koh, Olga Saukh, Alexander Ratner, Shuran Song, Hannaneh Hajishirzi, Ali Farhadi, Romain Beaumont, Sewoong Oh, Alex Dimakis, Jenia Jitsev, Yair Carmon, Vaishaal Shankar, and Ludwig Schmidt. Datacomp: In search of the next generation of multimodal datasets. *arXiv preprint arXiv:2304.14108*, 2023.
- [52] Gabriel Ilharco, Mitchell Wortsman, Ross Wightman, Cade Gordon, Nicholas Carlini, Rohan Taori, Achal Dave, Vaishaal Shankar, Hongseok Namkoong, John Miller, Hannaneh Hajishirzi, Ali Farhadi, and Ludwig Schmidt. Openclip, July 2021. URL <https://doi.org/10.5281/zenodo.5143773>.
- [53] Jonathan Krause, Michael Stark, Jia Deng, and Li Fei-Fei. 3d object representations for fine-grained categorization. In *Proceedings of the IEEE international conference on computer vision workshops*, pages 554–561, 2013.
- [54] Mircea Cimpoi, Subhansu Maji, Iasonas Kokkinos, Sammy Mohamed, and Andrea Vedaldi. Describing textures in the wild. In *Proceedings of the IEEE conference on computer vision and pattern recognition*, pages 3606–3613, 2014.
- [55] Patrick Helber, Benjamin Bischke, Andreas Dengel, and Damian Borth. Eurosat: A novel dataset and deep learning benchmark for land use and land cover classification. *IEEE Journal of Selected Topics in Applied Earth Observations and Remote Sensing*, 12(7):2217–2226, 2019.
- [56] Johannes Stallkamp, Marc Schlipsing, Jan Salmen, and Christian Igel. The german traffic sign recognition benchmark: a multi-class classification competition. In *The 2011 international joint conference on neural networks*, pages 1453–1460. IEEE, 2011.
- [57] Gong Cheng, Junwei Han, and Xiaoqiang Lu. Remote sensing image scene classification: Benchmark and state of the art. *Proceedings of the IEEE*, 105(10):1865–1883, 2017.

- [58] Jianxiong Xiao, Krista A Ehinger, James Hays, Antonio Torralba, and Aude Oliva. Sun database: Exploring a large collection of scene categories. *International Journal of Computer Vision*, 119:3–22, 2016.
- [59] Yuval Netzer, Tao Wang, Adam Coates, Alessandro Bissacco, Baolin Wu, Andrew Y Ng, et al. Reading digits in natural images with unsupervised feature learning. In *NIPS workshop on deep learning and unsupervised feature learning*, volume 2011, page 4. Granada, 2011.
- [60] Yann LeCun. The mnist database of handwritten digits. <http://yann.lecun.com/exdb/mnist/>, 1998.
- [61] Lucas Monteiro Paes, Dennis Wei, and Flavio Calmon. Selective explanations. *Advances in Neural Information Processing Systems*, 37:55562–55590, 2024.
- [62] Alex Krizhevsky. Learning multiple layers of features from tiny images. 2009. URL <https://api.semanticscholar.org/CorpusID:18268744>.
- [63] Adam Coates, Andrew Ng, and Honglak Lee. An analysis of single-layer networks in unsupervised feature learning. In *Proceedings of the fourteenth international conference on artificial intelligence and statistics*, pages 215–223. JMLR Workshop and Conference Proceedings, 2011.
- [64] Yifei Zhang, James Song, Siyi Gu, Tianxu Jiang, Bo Pan, Guangji Bai, and Liang Zhao. Saliency-bench: A comprehensive benchmark for evaluating visual explanations, 2025. URL <https://arxiv.org/abs/2310.08537>.
- [65] Kanglong FAN, Chen Ma, YIFAN PENG, Yuming Fang, and Kede Ma. Decision rules are in the pixels: Towards pixel-level evaluation of saliency-based XAI models, 2024. URL <https://openreview.net/forum?id=mKGXdsq7fD>.
- [66] Chih-Kuan Yeh, Cheng-Yu Hsieh, Arun Suggala, David I Inouye, and Pradeep K Ravikumar. On the (in) fidelity and sensitivity of explanations. *Advances in neural information processing systems*, 32, 2019.